Imaging of vortex states in mesoscopic superconductors

Goran Karapetrov[a)]
Material Science Division, Argonne National Laboratory, Argonne, Illinois 60439

Jan Fedor
Material Science Division, Argonne National Laboratory, Argonne, Illinois 60439 and Institute of Electrical Engineering, Slovak Academy of Sciences, Dúbravská cesta 9, 84104 Bratislava, Slovak Republic

Maria Iavarone
Material Science Division, Argonne National Laboratory, Argonne, Illinois 60439

M. T. Marshall
Center for Microanalysis of Materials, University of Illinois - Urbana-Champaign, Urbana, Illinois 81801

R. Divan
Center for Nanoscale Materials, Argonne National Laboratory, Argonne, Illinois 60439

(Received 10 May 2005; accepted 23 August 2005; published online 14 October 2005)

Enhanced vortex pinning in nanoscale-engineered superconductors increases the superconducting critical currents by orders of magnitude. Spatial imaging of vortices in these systems at high magnetic fields would provide further insight into the pinning mechanisms and enable development of high-pinning-strength materials. We have developed a novel method of fabricating atomically flat superconductor surfaces containing periodic array of normal metal pinning centers. Using scanning tunneling microscopy and spectroscopy, we map the local density of states in this heterostructure showing the vortex distribution at different applied magnetic fields. By increasing the applied magnetic field, the normal metal pinning centers accommodate several vortices per center until reaching the saturation point, beyond which new vortices get accommodated in the interstitial superconducting regions. The arrangement and pinning of the interstitial vortices is determined by the periodic pinning potential, and repulsive vortex-vortex interaction. © *2005 American Institute of Physics*. [DOI: 10.1063/1.2105993]

One of the main criteria determining the usefulness of superconductors is the amount of critical current that the material can carry without dissipation. Vortex movement or creep is the main source of power loss in both low-temperature and high-temperature superconductors (HTS). Reduction of the vortex creep at high magnetic fields and high temperatures can be achieved by inclusion of nonsuperconducting centers with sizes on the order of the vortex core. The pinning force exhibited by the pinning centers on the Abrikosov vortices can be formidable and it can lead to critical current enhancement that is several orders of magnitude. These improvements have been demonstrated in model systems such as superconducting thin films with anti-dot arrays[1] and in second generation superconducting HTS wires.[2] In order to understand the influence of the pinning centers on the vortex distribution and vortex dynamics in the superconductor, several real space imaging techniques have been utilized.[3,4] Most of these techniques are based on detecting the magnetic signature of the Abrikosov vortex and therefore have limited spatial resolution. Scanning tunneling microscopy (STM) measures the local density of states on the surface of the superconductor to resolve individual vortices. This leads to improved resolution in materials with smaller coherence length such as HTS. In order to take full advantage of the STM technique, one needs to meet rigorous requirements on surface quality. Surface roughness and the presence of passive adlayers have been an insurmountable problem. So far only limited success in STM vortex imaging has been accomplished in materials other than pristine single crystals.[5,6] Here we present a fabrication method that leads to well-controlled engineered superconducting surfaces containing periodic array of normal metal pinning centers. For the first time we present the STM vortex images in superconducting-normal metal heterostructures at magnetic fields that are up to 100 times of the matching field of the system and close to real application conditions. The described fabrication method opens possibilities to study vortex pinning and vortex dynamics in the presence of controlled nano-size pinning centers. Such studies are essential for understanding and predicting the superconductor current-carrying performance.

$NbSe_2$ single crystals were grown in evacuated quartz ampoules by an iodine vapor transport method.[7] Flat samples with sizes of up to $10\times10\times0.1$ mm^3 were characterized by x-ray, transport, and magnetization measurements. Superconducting quantum interference device magnetization measurements show typical superconducting transitions of 7.2 K with transition width of 10 mK. As-grown single crystals were cleaved to expose a clean flat surface. Using a focused beam of gallium ions (FEI DB-235) we etched a set of 1 μm deep parallel grooves spaced equidistantly 0.5 μm apart (Fig. 1). A second set of identical grooves, orthogonal to the original one, was inscribed in the same area producing an array of single crystal pillars [Fig. 1(e)]. Although the modulated surface looks smooth under high resolution scanning electron micrograph (SEM), we were not able to obtain superconductor-insulator-normal metal tunneling spectra by

[a)]Author to whom correspondence should be addressed; electronic mail: goran@anl.gov

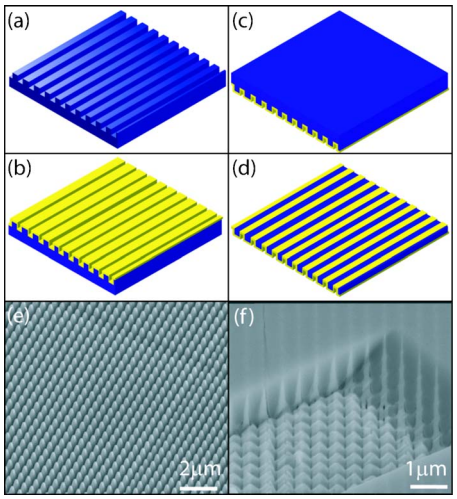

FIG. 1. (Color online) Microfabrication of submicron mesoscopic single crystal superconductors: high aspect ration FIB patterning (a) is followed by gold electroplating (b) with subsequent backside exposure (c) and cleaving (d). SEM micrographs show the $NbSe_2$ single crystal surface after performing FIB patterning with periodic structure containing a square array of pillars (e) and the surface and cross-sectional structure after the final cleavage step (f). At the bottom of the FIB milled box one can see the electroplated gold that penetrates the interstitials of the single crystal.

STM. It is most likely that the Ga ions and the debris from ion milling rapidly contaminate the STM tip.

To resolve the above problem, we proceeded with microfabrication by electroplating 2 μm of gold on the patterned surface. We used a Techni-gold 25E (Technic Inc.) electroplating solution at 40 °C, and current density 1 mA/cm^2. Gold sulfite $[Au(SO_3)_2]Na_3$ is the active ingredient and the solution operates at neutral *p*H. From atomic force microscopy measurements, a roughness of 11.88 nm (rms) was established to be typical for a 1-μm-thick gold layer obtained with this solution. Thermostating, magnet stirring, and continuous filtration during the deposition were used to control the deposition rate. After the electroplating step the undisturbed flat backside of the patterned single crystal of $NbSe_2$ was subsequently cleaved several times until the underlying etched/electroplated gold pattern was uncovered [Figs. 1(d) and 1(f)]. The latter procedure was performed in an inert atmosphere of He gas to avoid contamination of the freshly exposed $NbSe_2$ surface. This method produces a clean atomically flat $NbSe_2$ single crystal surface which is imbedded with laterally patterned gold islands. The sample was then immediately transferred into a low-temperature scanning tunneling microscope and cooled down to 4.2 K. This novel approach in fabricating patterned atomically flat single crystal surfaces free of surface contaminants is a key requirement for performing scanning tunneling spectroscopy imaging of vortices. A scanning electron micrograph of the heterostructure's cross section is shown in Fig. 1(f). By milling of the small area of the sample using focused ion beam (FIB), we expose the cross-sectional profile showing the interconnected $NbSe_2$ areas with protruding periodic gold islands.

A STM topographic image taken on a 1.4×2.0 μm^2 area shows that the crystal surface consists of atomically flat regions with elliptical gold islands [Fig. 2(a)]. The height profile shows that the apparent variation across the gold island is less than 1 nm. Using scanning tunneling spectroscopy we can measure the local conductance and thus determine the local density of states at every point on the surface.[8]

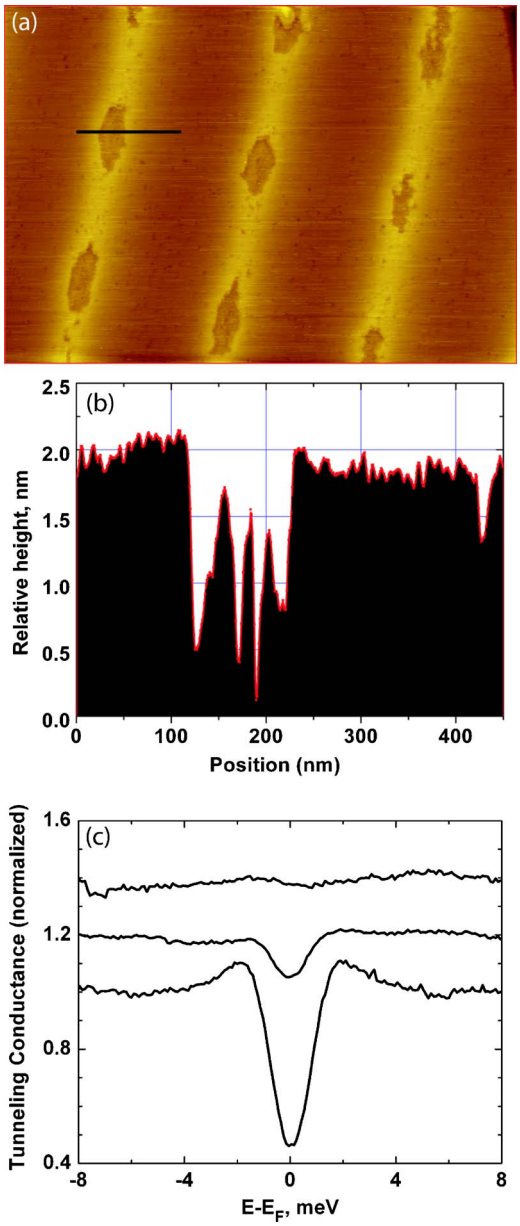

FIG. 2. (Color online) STM topography (2×1.4 μm^2) of the $NbSe_2$ single crystal surface with periodic array of elliptical gold pinning centers at 4.2 K (a). The apparent surface profile across the gold center (black line segment) shows variations that do not exceed 1 nm over 0.5 μm (b). STM spectroscopy performed along the black segment line show superconducting tunneling conductance spectra on the $NbSe_2$ surface area that gradually transforms into flat normal metal conductance spectra recorded in the center of the gold island (c).

A typical set of superconducting tunneling spectroscopy spectra along a line passing through the center of the Au island is shown in Fig. 2(c). The tunneling conductance spectra taken between the holes show the typical superconducting gap of $NbSe_2$ at 4.2 K with a superconducting energy gap value of 1.0 meV. On the other hand, the spectrum taken in the middle of the ellipse shows gapless conductance of a normal metal—a signature of the presence of gold. The smooth transition in the conductance spectra when approaching the gold area is due to the superconducting proximity effect between the normal metal (Au) and superconductor ($NbSe_2$). The superconducting correlations propagate into the normal metal and induce a finite gap in the local excitation spectra.[8]

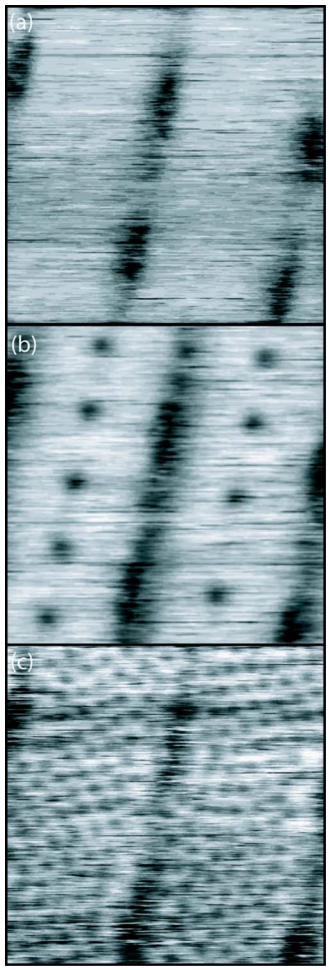

FIG. 3. Images of vortex configurations in a square array of normal metal elliptical holes at zero applied magnetic field (a) and matching magnetic fields of $H=10H_0$ (b) and $H=72H_0$ (c) where H_0 is the matching field of the pattern equal to 82.8 Oe. The images were recorded using current image tunneling spectroscopy on an area of 1.25×1.25 μm^2 at 4.2 K.

Visualizing vortices by STM is based on the fact that there are gap states inside a vortex core, and therefore the quasiparticle tunneling conductance spectrum exhibits an increase around the Fermi energy. The main difference in conductance curves inside and outside the vortex core is at the Fermi level ($V_{bias}=0$ V) and near the superconducting gap peak ($V_{bias}=\pm2.0$ meV). We performed a conductance map at $V_{bias}=+2.0$ meV which resulted in superconducting areas having higher conductance (bright areas) than the gapless regions (dark areas). A typical local density of states map in zero applied magnetic field is shown in Fig. 3(a). The image shows that the periodic array of elliptical islands has a lower conductance at 2 meV consistent with the spatially dependent tunneling spectra across the normal areas shown in Fig. 2(c). The square periodicity of the array of submicron gold islands forms an ideal periodic trapping potential for the Abrikosov vortex lattice.[1,9] The first matching field, a condition when each island contains one magnetic flux quantum, is 82.8 Oe. When magnetic field is applied perpendicular to the surface of the $NbSe_2$ superconductor the Abrikosov vortices penetrate the sample. They are first accommodated inside the normal islands that act as excellent pinning centers. The size of the islands is such that each island could accommodate up to six Abrikosov vortices.[10] As magnetic field is increased beyond the sixth matching field we can resolve the individual Abrikosov vortices that are accommodated in the interstitial regions. The Abrikosov vortices are positioned such as to minimize the total energy of their repulsive interaction with circulating screening currents around each normal island as well as the Meissner currents flowing along the perimeter of the sample. Due to the low intrinsic pinning of the single crystal material the vortex distribution takes close to equilibrium distribution even far below the critical temperature. Periodicity of the interstitial Abrikosov vortices is fully determined by the symmetry of the periodic pinning potential of the gold islands. When the applied magnetic field increases such that inter-vortex spacing becomes much smaller than the period of the pinning array, the vortex-vortex interaction becomes dominant. In equilibrium case this leads to the classical solution—arrangement of the vortices in triangular lattice[11] as we observe in the interstitial areas of the crystal surface [Fig. 3(c)]. Our results resemble molecular dynamics simulations on similar systems with periodic pinning potential.[12]

In conclusion, we have developed a novel method of fabricating atomically flat single crystal superconductor/normal metal heterostructures containing periodic array of normal metal pinning centers. STM images at low temperatures and high magnetic fields show the changing vortex distribution at different applied magnetic fields. Increasing the applied magnetic field leads to increased number of vortices in the sample. The normal metal pinning centers trap several vortices per center until reaching the saturation point, beyond which new vortices get accommodated in the interstitial superconducting regions. The forces from the circulating Meissner currents and the currents around the multiquanta vortices in the pinning centers determine the arrangement of interstitial vortices.

The authors would like to acknowledge M. Moldovan (Northwestern University) and D. Rosenmann (Argonne) for their help with sample preparation and V. Vlasko-Vlasov (Argonne) and M. Zalalutdinov (Cornell) for useful discussions. Part of this work was carried out at the Center for Microanalysis of Materials, University of Illinois at Urbana-Champaign, which is partially supported by the U. S. Department of Energy under Grant No. DEFG02-91-ER45439. This work has been supported by the U.S. DOE, BES-Material Sciences under Contract No. W-31-109-ENG-38.

[1] M. Baert, V. V. Metlushko, R. Jonckheere, V. V. Moshchalkov, and Y. Bruynseraede, Europhys. Lett. **29**, 157 (1995).
[2] R. F. Service, Science **308**, 348 (2005).
[3] A. Oral, S. J. Bending, and M. Henini, Appl. Phys. Lett. **69**, 1324 (1996).
[4] G. J. Dolan, F. Holtzberg, C. Field, and T. R. Dinger, Phys. Rev. Lett. **62**, 2184 (1989); H. F. Hess, R. B. Robinson, and J. V. Waszczak, Phys. Rev. Lett. **64**, 2711 (1990).
[5] T. Nishizaki, A. M. Troyanovski, G. J. C. van Baarle, P. H. Kes, and J. Aarts, Physica C **388**, 777 (2003).
[6] G. J. C. van Baarle, A. M. Troyanovski, P. H. Kes, and J. Aarts, Physica C **369**, 335 (2002).
[7] C. S. Oglesby, E. Bucher, C. Kloc, and H. Hohl, J. Cryst. Growth **137**, 289 (1994).
[8] M. Tinkham, *Introduction to Superconductivity* (Krieger, Malabar, 1975).
[9] V. V. Moshchalkov, M. Baert, V. V. Metlushko, E. Rosseel, M. J. van Bael, K. Temst, R. Jonckheere, and Y. Bruynseraede, Phys. Rev. B **54**, 7385 (1996).
[10] G. S. Mkrtchyan and V. V. Shmidt, Sov. Phys. JETP **34**, 195 (1972).
[11] A. A. Abrikosov, Sov. Phys. JETP **5**, 1174 (1957).
[12] C. Reichhardt, G. T. Zimanyi, and N. Gronbech-Jensen, Phys. Rev. B **64**, 014501 (2001).